Aerodynamics of a Uranus Aerocapture System Using a Mars-Heritage Entry Vehicle

Eli R. Shellabarger*, James B. Scoggins†, Andrew D. Hinkle‡, Rohan G. Deshmukh*, Soumyo Dutta§
NASA Langley Research Center, Hampton, VA 23681, USA

Sarah Agam¶, Mihirkumar Patel‡
ViGYAN, Inc., Hampton, VA 23666, USA

Aerodynamic characteristics of an aerocapture system intended to deliver a flagship-class orbiter and probe planetary science mission to Uranus are presented. The aeroshell of the Mars Science Laboratory and Mars 2020 entry vehicles is proposed as a baseline for this system to reduce the amount of necessary technology development. Direct Simulation Monte Carlo and Navier-Stokes computational fluid dynamics solutions are used to characterize the aerodynamic performance of the Mars-heritage vehicle for aerocapture flight at Uranus. These results are incorporated into an aerodatabase for use in six degree-of-freedom trajectory studies and mission design. Updates are made to the Mars-heritage aerodynamic uncertainty model based on observations in the Uranus-specific computational data to ensure the model is conservatively bounding for the proposed flight space. Necessary modifications to the aeroshell for system packaging are found to have minimal effect on aerodynamic performance. The resulting aerodatabase and uncertainty model are used to show the existing Mars-heritage entry vehicles have sufficient aerodynamic performance to achieve required control margin for Uranus aerocapture.

I. Nomenclature

α	=	Angle of Attack, deg
α_T	=	Total Angle of Attack, deg
β	=	Angle of Sideslip, deg
C_A	=	Axial force coefficient
C_N	=	Normal force coefficient
C_Y	=	Side force coefficient
C_l	=	Roll moment coefficient
C_m	=	Pitch moment coefficient
C_n	=	Yaw moment coefficient
D	=	Vehicle Diameter, m
γ	=	Ratio of Specific Heats
h	=	Altitude, m
Kn	=	Knudsen number
L/D	=	Lift-to-Drag Ratio
λ	=	Mean Free Path, m
M	=	Mach number
$M.W.$	=	Molecular Weight, kg/kmol
μ	=	Dynamic Viscosity, Pa $\cdot$ s
n	=	Number Density, $1/\text{m}^3$
$\mathbb{R}$	=	Range (Statistics)

*Aerospace Engineer, Atmospheric Flight and Entry Systems Branch, AIAA Member.
†Research Aerospace Engineer, Aerothermodynamics Branch, AIAA Member.
‡Aerospace Engineer, Aerothermodynamics Branch, AIAA Member.
§Aerospace Engineer, Atmospheric Flight and Entry Systems Branch, Associate Fellow.
¶Aerospace Engineer, Aerothermodynamics Branch.

ρ = Mass Density, kg/m^3
S_μ = Sutherland Constant, K
σ = Standard Deviation (Statistics)
T = Temperature, K

II. Introduction

Ice Giant planets, and Uranus in particular, have been identified as the highest priority destination for a new flagship planetary science mission in the 2020-2030s time frame by the Planetary Science Decadal Survey released by the National Academies of Science in 2022 [1]. Uranus Orbiter and Probe (UOP), the baseline mission study considered by this Decadal Survey, would need to launch in the early 2030s and dedicate approximately two-thirds of the total mass to propellant in order to reach Uranus ahead of its 2049 equinox, a goal of the scientific community driving interest in this mission [2]. Given that work on such a mission has yet to officially begin within a decade of the launch date (not to mention anticipated budgetary constraints in the coming years), it can be reasoned that such a flagship mission would face heavy constraints on development timeline from the outset, casting doubt on the ability to launch such a mission on time.

Aerocapture offers a solution to reach a science orbit at a planetary body in a single orbital pass by utilizing the forces generated from atmospheric flight to decelerate from interplanetary speeds into a desired, captured orbit. The concept of operations for an aerocapture maneuver at Uranus is depicted in Figure 1. For a flagship Uranus mission, it has been shown that aerocapture reduces mass and interplanetary travel time, making later launches for such a mission possible and allowing for a more flexible launch schedule [3–6].

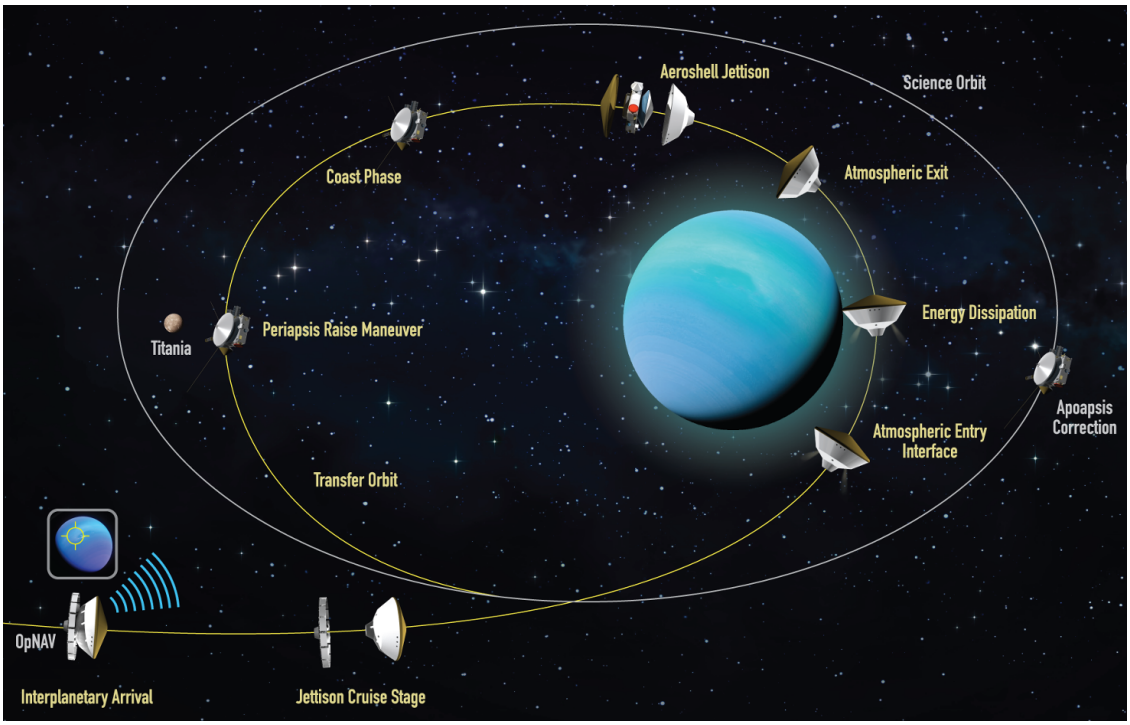

Fig. 1 Uranus Aerocapture Concept of Operations [5]

A key performance metric for an aerocapture system is the lift-to-drag ratio, L/D, which provides a measurement for the system's control authority during the deceleration period. A higher L/D enables greater control authority, through which the system can achieve greater success margins for the maneuver. While previous efforts have designed novel Mid-L/D ($0.6 \lesssim L/D \lesssim 0.8$) systems for aerocapture at Ice Giants [7, 8], technology development remains an obstacle for a new system to be selected for use on a flight mission. Designing an aerocapture system around a Low-L/D ($L/D \lesssim 0.3$) heritage flight system reduces concerns and costs associated with technology development, while also reducing uncertainties by re-purposing a known system. Since there are no prior missions with atmospheric

flight at Uranus, with the closest example being the sole flight of the Galileo probe at Jupiter [9], the next best option is reanalysis of a previously flown system from another planet under Uranus conditions. The geometry of the Mars Science Laboratory (MSL) entry vehicle (EV) [10, 11], which was flown again for Mars 2020 [12, 13], has been chosen for Uranus aerocapture given its repeated flight heritage use in flying a lifting trajectory on multiple planetary exploration missions to Mars.

Previous work has explored the overall feasibility and aerodynamic implications of atmospheric flight at Uranus for a Low-L/D aerocapture system that packages the UOP system [5, 14, 15]. Additional prior work has considered the aerothermal environments and thermal protection system of the concept [16, 17]. The current work builds on this understanding as part of a NASA Space Technology Mission Directorate (STMD) activity [18] to create an aerodynamic model of an aerocapture system designed around the MSL EV for atmospheric flight at Uranus on an aerocapture trajectory.

III. Geometry and Reference Frames

Two aerocapture system configurations were assessed in the current work, shown in Figure 2. The first configuration is a proportional scaling of the MSL EV from 4.5 m to 5 m maximum diameter. This configuration was found to be capable of packaging the UOP payload with scale size being the only modification [15]. The bulk of the subsequent analysis has been performed on this first configuration. However, the 5 m scale of this configuration is expected to exceed the payload constraints of current day launch vehicles. For that reason, a second configuration was considered with a 4.57 m maximum diameter, which is expected to satisfy presently available launch vehicle fairing constraints. The 4.57 m configuration retains the same heatshield geometry (scaled) as the MSL EV, but requires a slight modification to the backshell to fit the UOP payload [19]. It is worth noting that a similar backshell growth was seen on the MSL EV [10], which originally used a backshell that more closely resembled the Mars Viking EV [20], and was found to have little to no significant effect [21]. Analysis has been conducted in the current work to quantify the effects of these deviations from the MSL EV in the 4.57 m configuration, and is discussed in Section VI.D.

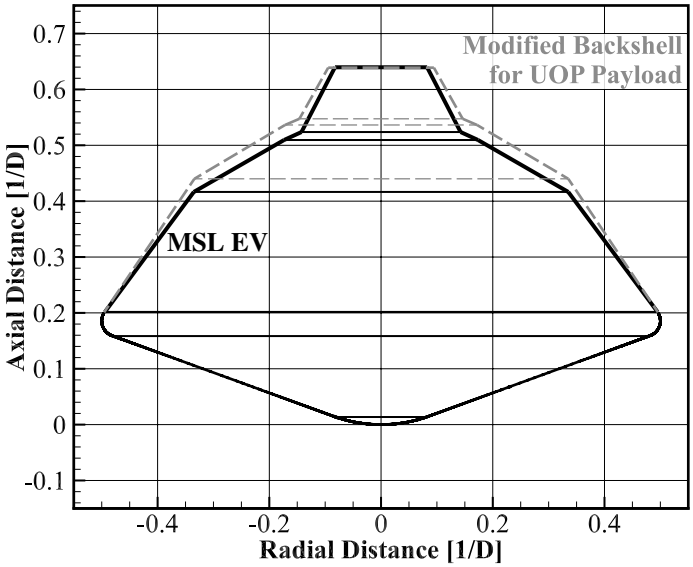

Fig. 2 MSL EV and Required Backshell Modification for Uranus Orbiter and Probe Packaging

A consistent coordinate frame description was used on both configurations, and is depicted in Figure 3. Given all geometries considered have an outer mold line (OML) that is axisymmetric about their center line (CL), the total angle of attack, α_T, as defined in Equation 1, is used as the state variable for vehicle orientation when showing axisymmetric data.

$$\alpha_T = \arccos\left(\cos\left(\alpha\right)\cos\left(\beta\right)\right) \tag{1}$$

However, when a radial offset to the center of gravity (CG) is used to trim the vehicle, data are expressed in terms of

a state variable which sees the non-zero trim angle, which in the current work is assumed to be the angle of attack, α. This trim flight state is intended to achieve a $L/D \simeq 0.25$ at an attitude of $16^\circ \lesssim \alpha_T \lesssim 18^\circ$. This is in-family with the flight profile of MSL and Mars 2020. For the purposes of the current documentation, the CG to achieve this trim condition was assumed to be located at:

$$\langle x/D, y/D, z/D \rangle_{cg} \Big|_{bc} = \langle 0.235, 0.000, -0.026 \rangle$$

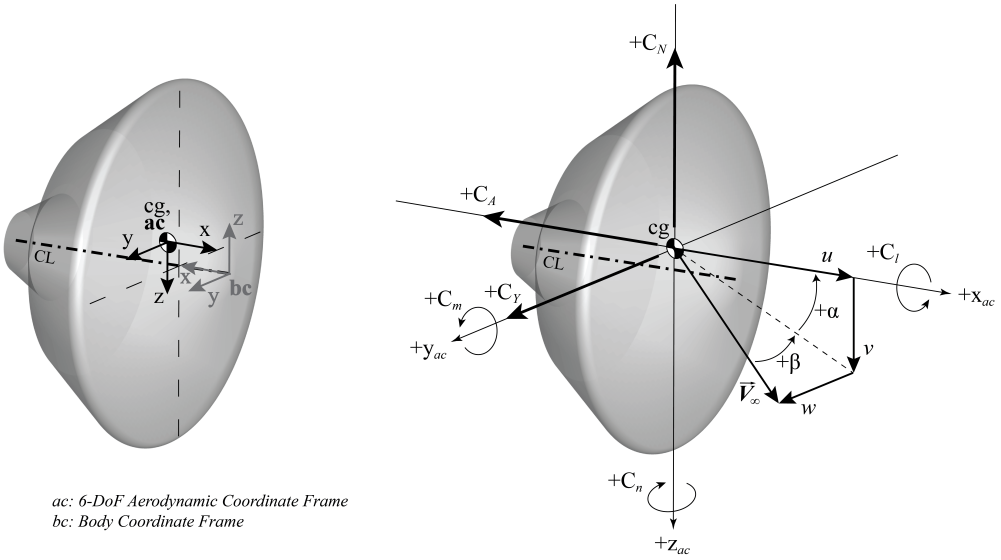

Fig. 3 Aerodynamic Coordinate Frames (Exaggerated)

IV. Methods

A variety of computational fluid and gas dynamics solvers were used to characterize the aerodynamic properties of the geometries described in Section III while in flight through Uranus conditions. Portions of the data generated were used in conjunction with engineering analysis and judgement to develop an aerodynamic database for the purposes of flight trajectory and performance analysis. The following section describes the methods used to define aerodynamic performance.

A. MAP

The Multiphysics Algorithm with Particles (MAP) [22] code is a Direct Simulation Monte Carlo (DSMC) tool used to calculate aerodynamic and thermodynamic data in the rarefied/transitional regime ($Kn > 10^{-3}$) for the current work. MAP is an object-oriented/data-oriented code written in C++ that uses new algorithms which include features such as separate collision and sampling cells, automatic adaptive grid, variable time steps, a modified no-time counter procedure for collisions, and discontinuous and event driven physical processes to improve physical accuracy and computational efficiency. An object-oriented program creates a modular structure that allows for easy modification of programs within MAP. Data-oriented code focuses on data maintenance during program execution.

MAP is a multidimensional adaptive Cartesian implementation of DSMC that allows for local adaptions to spatial and temporal requirements in the flow field and uses the Cartesian grid system for particle collision, movement, and sampling procedures. MAP was designed with the high energy physics of re-entry in mind and allows for electronic energy relaxation (in addition to rotational and vibrational) and includes a quasi-neutral ionized flow model that tracks electrons along with their associated ions. In addition, all particle properties have been tuned* [23] to more closely

*Liechty, D. and Swaminathan-Goplan, K., Personal Communication, 20 November 2020

match the viscosity and thermal conductivity resultant from the collision integrals used in the LAURA CFD algorithm, discussed in Section IV.B.

Computations in the current work utilized a half-body symmetric model of the scaled 5 m MSL EV described in Section III. MAP cases were not run on the final 4.57 m Uranus aerocapture configuration. The surface grid of this model is shown in Figure 4. The size of the bounding box depended on the condition-specific value of Knudsen number, $Kn = \lambda/D$, which uses the aerocapture system body diameter as the reference length. At high altitudes where the Kn is largest, the shock is diffused, and a large bounding box is required. At conditions deeper into the atmosphere, the shock is more pronounced, and the grid adapts multiple times to accurately capture the flow physics, resulting in a smaller bounding box. The shock can be seen in Figure 5.

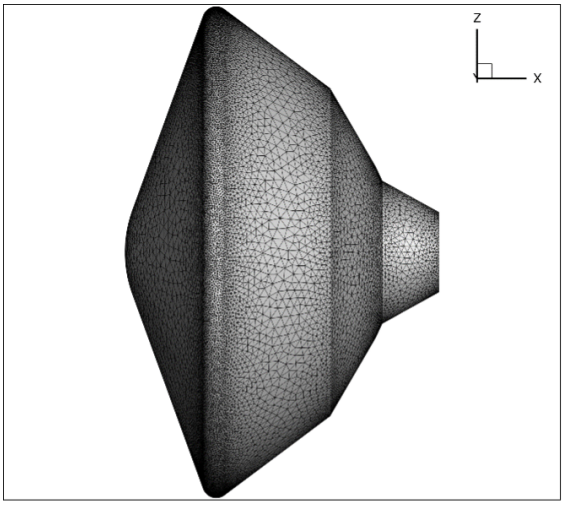

Fig. 4 MAP Surface Grid

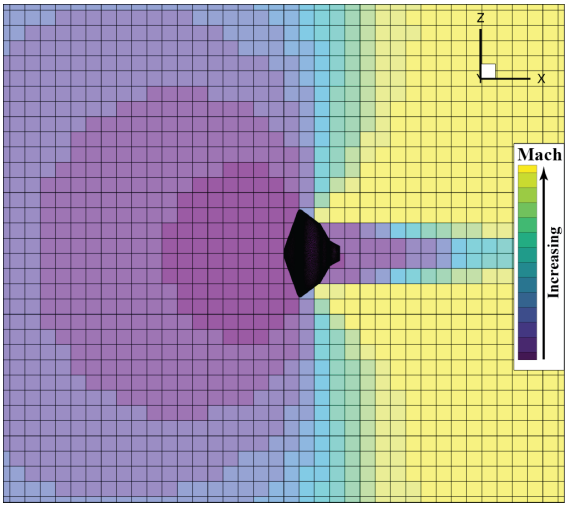

(a) MAP Solution at $h \approx 3.8 \times 10^6$ m, $Kn \approx 6.1 \times 10^2$

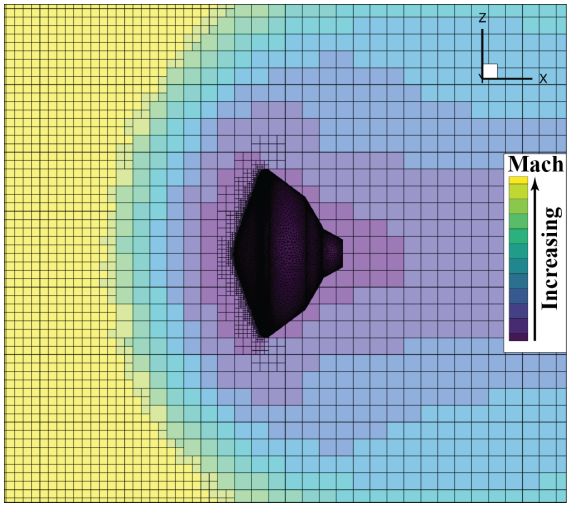

(b) MAP Solution at $h \approx 7.6 \times 10^5$ m, $Kn \approx 5.4 \times 10^{-2}$

Fig. 5 MAP Solutions with Adapted Volume Grids, $\alpha_T = 0°$

Two primary chemistry models and a third sensitivity model were run with MAP for the current study to bound the effects of atmospheric variations expected within Uranus' atmosphere [24]. Cases were run in each model for a matrix of number density and total angle of attack. The first set of cases used a two-gas model comprised of atomic hydrogen (H) and molecular hydrogen (H_2). The freestream in the pure hydrogen model is entirely molecular hydrogen, representative of Uranus' upper atmosphere. The second model, mixed hydrogen-helium (H_2, He, H), added helium (He) to the former

model. Helium is expected to be found at lower altitudes at Uranus, and the predicted equilibrium mixture mole fractions of 0.85 H_2 and 0.15 He were used for the freestream conditions. A subset of mixed hydrogen-helium cases were run with a third model to explore ionized mixed gas effects (H_2, He, H, H^+, He^+, e^-) at a subset of attitude angles.

Solution convergence of the completed runs was determined by inspection of local cell Knudsen values, Kn_{Cell}, along with force and moment convergence. DSMC grid adaption is viewed as improved over previous work [14], where some cases saw poor adaption leading to larger variance in resulting coefficients than the current work. Computation of the final achieved Knudsen number in each DSMC solution in the current work is also viewed as improved. While prior work utilized legacy collision data to compute Kn, updated collision data consistent with underlying models within MAP are used for the calculation of Knudsen number in the current work[†].

B. LAURA / HARA

The NASA Langley Aerothermodynamic Upwind Relaxation Algorithm (LAURA) [25–27] and Hypersonic Aerothermodynamic Radiation Algorithm (HARA) [28] were used to compute aerothermodynamic data in the hypersonic continuum regime for the current work. LAURA solves the thermochemical nonequilibrium, multicomponent Navier-Stokes equations [29] on a cell-centered, structured multiblock discretization. Second-order accuracy is obtained using the symmetric total variation diminishing (TVD) scheme by Yee [30] with point or line-implicit pseudotime integration. Radiation calculations were performed using the HARA code, which is fully coupled within LAURA. HARA provides coupled volume radiation source terms through the tangent-slab approximation and accurate surface radiative heating calculations using ray-tracing at surface mesh points [31]. All results are obtained using a two-temperature thermochemical nonequilibrium model with six species, including H_2, He, H, H^+, He^+, and free electrons. A five-reaction chemical mechanism was employed based on rates provided by Park [32] and Fujita [33], as compiled by Scoggins [16]. Fully-catalytic, radiative equilibrium boundary conditions were employed at the walls. The main data products from the LAURA solutions are the static force and moment coefficients, and the convective heat transfer to the vehicle surface as a result of hot gases in the boundary layer.

LAURA cases were run on block-structured forebody-only domains of the scaled 5 m MSL EV and utilized shock-aligned grid adaptation. A shock-adapted forebody-only domain at a representative condition is shown in Figure 6. Backshell effects were neglected in the current work as their contributions to the aerodynamic performance are small. This is consistent with the assumptions of prior planetary entry vehicles in this regime. On previous Mars missions, forebody-only data were combined with a base pressure correction to the static coefficients where needed [21], and a similar approach could be used to augment the current data if sufficient data was available to inform a base pressure correction. However, this correction is expected to be small at the high-hypersonic Mach regime ($M \simeq 30$) of interest in the current work.

C. FUN3D

The NASA Fully Unstructured Navier-Stokes in Three Dimensions (FUN3D) code was used to analyze configuration related effects in the hypersonic continuum regime for the current work. FUN3D is a second-order, node-centered, unstructured CFD solver with a variety of models and fidelity that can be tailored to a user's needs. While FUN3D's generic gas path supports computations like those described in Section IV.B, FUN3D's compressible gas path, which applies the assumption of a compressible and calorically perfect gas, was utilized here. Utilizing calorically perfect assumptions has clear inaccuracies when modeling hypersonic aerodynamics that depend on reacting gas physics expected at such flight conditions. However, the calorically perfect solutions still give useful intuition for the pressure-dominated forces and moments the system would experience between configurations as used in the current work.

The Sketch-to-Solution (S2S) process [34] was utilized to automate the creation and adaptation of grids. The underlying geometries used were the scaled 5 m MSL EV and the final 4.57 m Uranus Aerocapture configuration as described in Section III. S2S predictions of the MSL EV at supersonic wind tunnel conditions have compared favorably to experimental data [35]. Full-body solution-adapted anisotropic tetrahedral grids were started from initial node counts of 5.0×10^5, and after 22 cycles of grid adaption and refinement, resulted in final grids with a node count on the order of 6.4×10^6. Total enthalpy was used as the adaption metric in these solutions. A representative solution is shown in Figure 7.

FUN3D models in this work used the dissipative low-diffusion flux-splitting scheme (DLDFSS) with a van Albada limiter, isothermal walls ($T_{wall} = 500$ K), and a laminar viscosity model. To model Uranus' H_2, He continuum

[†]Liechty, D., Personal Communication, 24 September 2024.

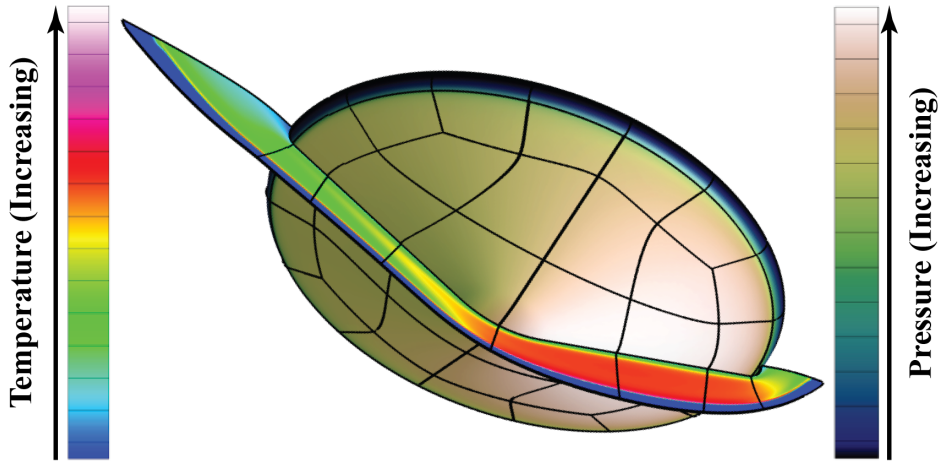

Fig. 6 LAURA Forebody-Only Adapted Solution Domain, $\alpha_T = 17.5°$

freestream in FUN3D, solver reference properties were modified to representative gas properties. Molecular weight was assumed to be $M.W. = 2.31\,\mathrm{kg\,kmol^{-1}}$. The ratio of specific heats was assumed to be $\gamma = 1.35$ nominally based on observations from prior LAURA simulations [14]. Additional effects of varying the ratio of specific heats based on pre- and post-shock conditions was also considered, but are only discussed in a limited manner in the current work due to outstanding questions regarding the physics modeled by making this assumption. A custom Sutherland Law fit was used to model fluid viscosity, developed as a product of corresponding aerothermal analysis [16]. Fitting the form of Equation 2 as used in FUN3D [36] gives $\mu_{ref} = 9.53 \times 10^{-6}\,\mathrm{Pa \cdot s}$, $T_{ref} = 273\,\mathrm{K}$, and $S_\mu = 427.17\,\mathrm{K}$.

$$\mu = \mu_{ref} \frac{T_{ref} + S_\mu}{T + S_\mu} \left(\frac{T}{T_{ref}} \right)^{3/2} \tag{2}$$

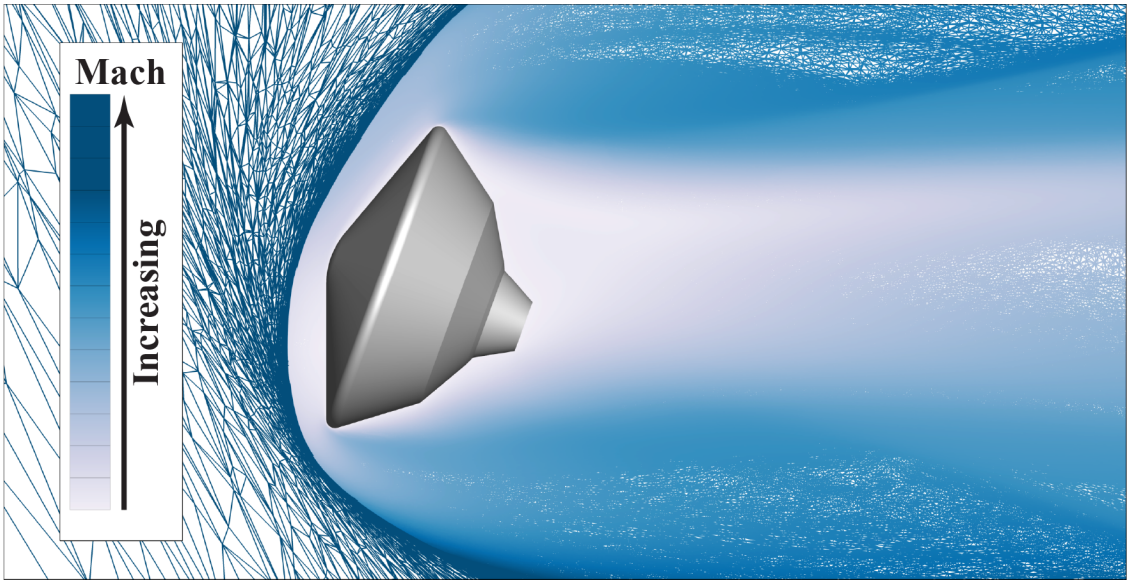

Fig. 7 FUN3D Adapted Grid Solution at Peak Dynamic Pressure, $\gamma = 1.35$, $\alpha_T = 20°$

V. Computational Data

The methods in Section IV were used to produce computational data on the geometries in Section III. The atmospheric conditions used to generate these data were obtained from evolving design reference trajectories. Solutions were run for these inputs based on the aerodynamic regime; DSMC for free molecular and transitional regime calculations, and reacting gas Navier-Stokes for hypersonic continuum regime calculations.

A. Reference Trajectories

All computational data in the current work were prescribed using conditions extracted from reference trajectories which evolved over a series of design analysis cycles (DACs). Each new set of computational data was run using the most recently available trajectory information at the time it was prescribed, and the conditions at which MAP and LAURA solutions were run are compared to three DAC trajectories in Figure 8. This creates a disconnect in the available data as they were prescribed from slightly different trajectories as the mission concept evolved. It can be seen in Figure 8 that the DAC2 trajectory on which MAP solutions are based sees a smaller reduction in speed compared to the DAC3 trajectory on which LAURA solutions are based. Meanwhile, the more recent DAC4 trajectory then appears to fall in the space between these trajectories. Given time constraints and required resources to further populate the potential trajectory space, along with previous analysis showing that aerodynamic properties show little sensitivity to deceleration effects in the expected flight regimes for Uranus Aerocapture applications [14], additional points in the trajectory space were not added. Handling of any uncertainty introduced by this decision are considered in Section VI.A. However, this approach is considered adequate for the conceptual study nature of the current work.

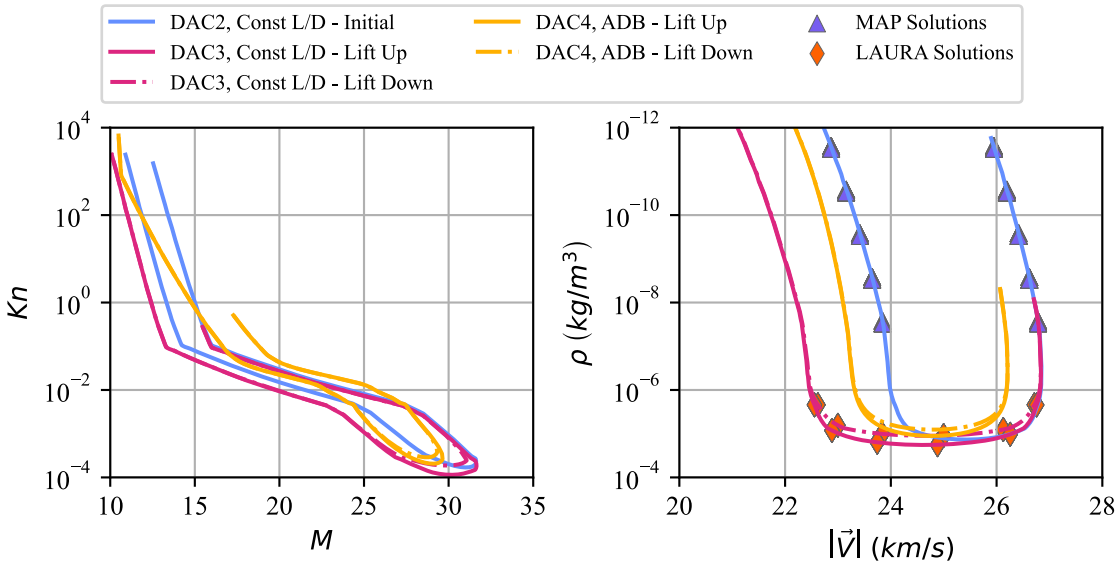

Fig. 8 Reference Trajectory Space

B. Rarefied Aerodynamic Data

Rarefied aerodynamic calculations using MAP as described in Section IV.A were completed to predict the aerodynamic properties in the transitional and free molecular regimes for flight in Uranus aerocapture conditions. Conditions were prescribed as a matrix of number density to target order of magnitude changes in Kn with sweeps in total angle of attack at each density point. Freestream velocity and temperature were set to the corresponding values extracted from the DAC2 reference trajectory described in Section V.A. Models of pure-hydrogen and an equilibrium blend of hydrogen-helium were run to account for variations in atmospheric composition. Limited additional runs were made to determine if ionization effects were significant at attitudes of $\alpha_T = 0°, 20°$. Additional large total angles of attack were computed for high-Kn conditions to bound modeling for cases where near-exoatmospheric maneuvering may result in high-α_T conditions. The force and moment coefficient data of these computations are plotted in Figure 9.

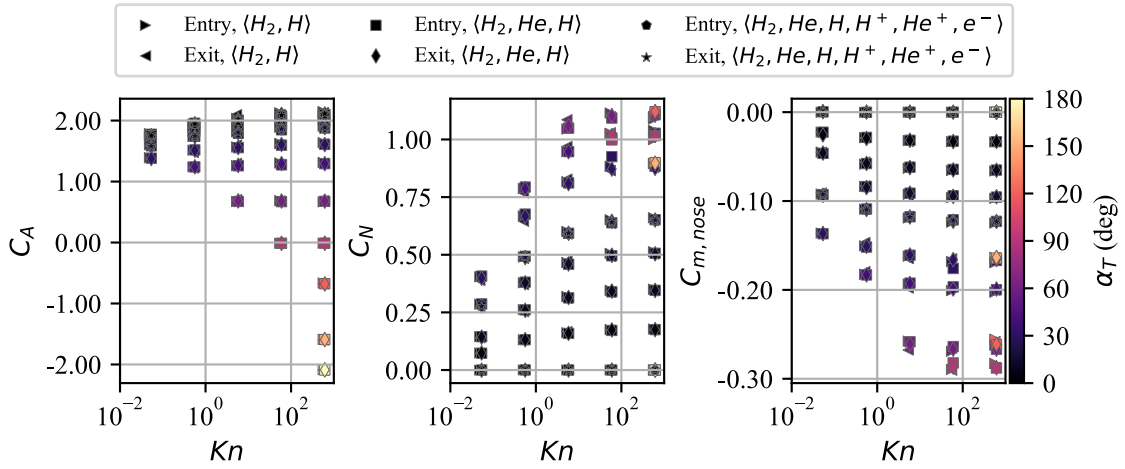

(a) All Attitudes

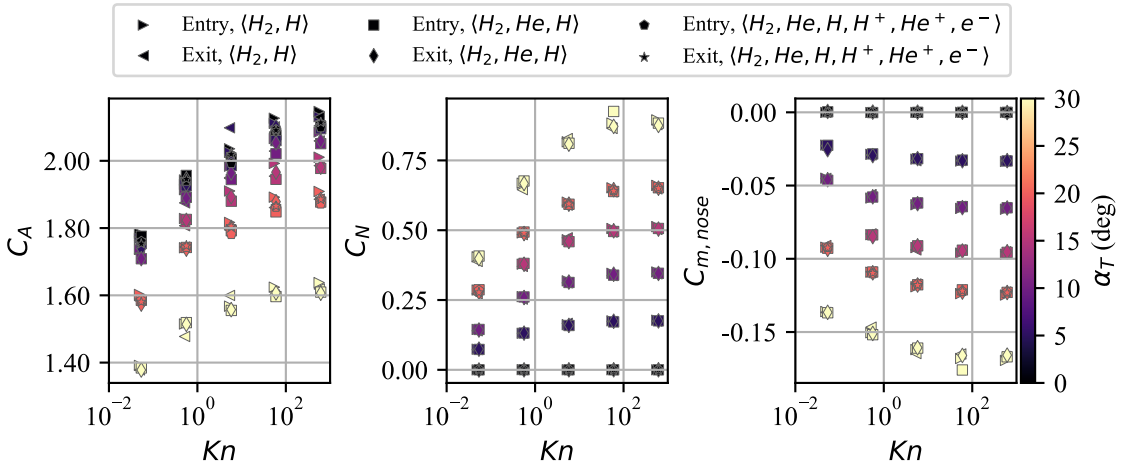

(b) Near-Trim Attitudes

Fig. 9 MAP Rarefied Solutions – Force and Moment Data

C. Continuum Aerodynamic Data

Calculations using LAURA as described in Section IV.B were completed to predict the aerodynamic properties in the continuum regime. Cases were run on DAC3 lift-up and lift-down trajectories, which bound the navigable flight space. Six conditions were run for each trajectory: two points for continuum entry and exit ($Kn = 10^{-3}$), one point at the peak dynamic pressure condition, and three points spaced evenly in time between the first three points (one before peak dynamic pressure, two after). A total angle of attack sweep was run for each of these conditions, which prescribed the corresponding velocity, mass density, and temperature. These cases used a constant equilibrium hydrogen-helium gas mixture, which included ionization. The force and moment data of these computations are plotted in Figure 10.

VI. Aerodynamic Characterization

The aerodynamic characterization of the MSL EV based aerocapture system in flight at Uranus is presented. Computations in Section V saw the largest variation in forces and moments due to Knudsen number and total angle of attack. The computational data were used to created a reduced set of nominal coefficients which reconcile the aerodynamic properties of the system as a function of these two primary variables. Uncertainties associated with these nominal coefficients were developed to bound the remaining variations in the computational data. The reconciled data are compared against Mars heritage data to validate the intended flight system legacy is maintained. The data are then used to formulate an aerodynamic database which can be integrated into flight mechanics analysis. The effects of

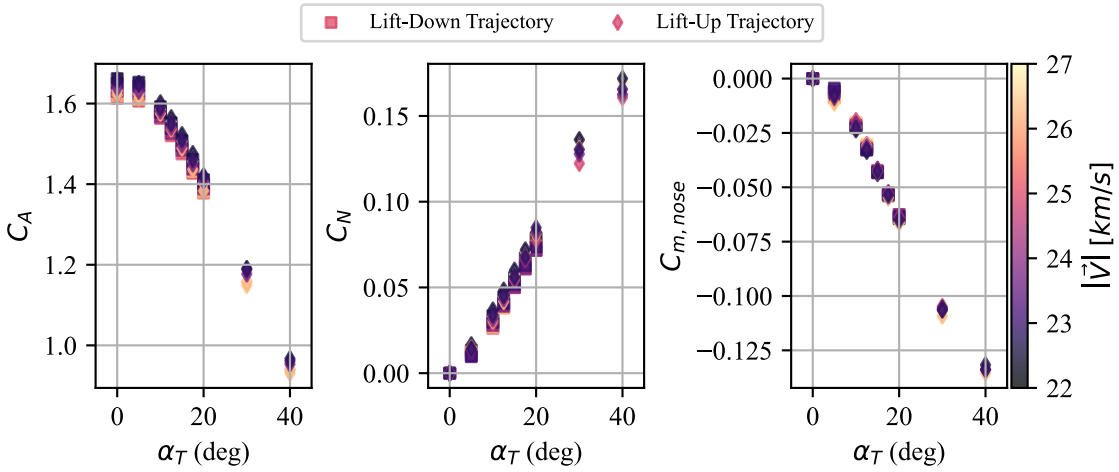

Fig. 10 LAURA Forebody-Only Continuum Solutions – Force and Moment Data

sensitivity to the backshell shape and dynamic damping are also considered.

A. Reconciled Static Aerodynamics

The available computational data show that for a given Knudsen number and total angle of attack, aerodynamic coefficients do not differ significantly. This section details the reconciliation of the available data as a function of these two variables. Uncertainties were formulated which capture the remaining small variations observed in the data. The reconciled aerodynamics are used to formulate the nominal aerodatabase described in Section VI.C, and the uncertainties are used in Section VII.

1. Rarefied

The aerodynamic data computed by MAP in Section V.B cover a wide range of conditions and gas models. This not only helps encompass the effects of an altitude-dependent gas composition and large reduction of velocity over the course of atmospheric flight, but also aerocapture-specific considerations such as the fact that the transitional regime is flown through twice – once on atmospheric entry prior to continuum hypersonic flight, and once again at notably lower velocities once the aerocapture system exits the atmosphere. This adds additional considerations for non-monotonic aerodynamics with respect to variables such as the Knudsen number. However, it can be seen in Figure 9 that there is very little variation between runs other than that caused by differences in Knudsen number and total angle of attack for the given flight conditions. This means effects such as velocity magnitude differences between entry and exit portions of aerocapture, change in gas composition with altitude, and effects of ionization can be characterized as secondary effects and captured in the uncertainties for the current work. This was leveraged in the reconciliation of the available computational data from MAP.

The available rarefied data for entry and exit conditions using the H_2, H and H_2, He, H gas models were averaged together to create a monotonic set of data with independent variables of Kn and α_T. Given the limited samples at each condition point, point-specific uncertainty (3σ) in coefficient values was approximated as the range, $\mathbb{R}_C\,(Kn, \alpha_T)$, of the observed values given they are prescribed from conditions representative of bounding cases. Additional conservatism was then added to this approximation of uncertainty by using the maximum observed range of the static aerodynamic coefficient for all Kn-α_T condition pairs; i.e., $U_C = \max(\mathbb{R}_C)$. The conservatism of this approach was limited by only querying uncertainties from α_T values that are near trim, defined as $\alpha_T < 30°$, to avoid large angle data far from the trim point driving conservatism in the uncertainties of the trim flight data. Ionized data from the H_2, He, H, H^+, He^+, e^- model was not included in the averaged coefficient values as they were only available at specific angles of attack, but was included in the uncertainty formulation. For moments, uncertainty estimates were calculated at the CG given this is the point about which uncertainties are typically applied in flight trajectory analysis. The reconciled rarefied aerodynamic data are shown with uncertainties in Figure 11.

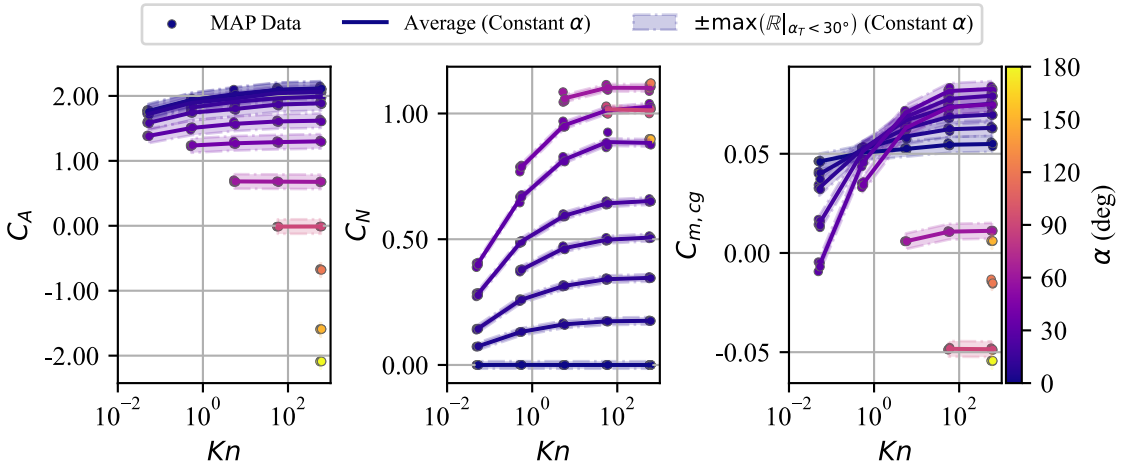

(a) Axial Force – All Attitudes

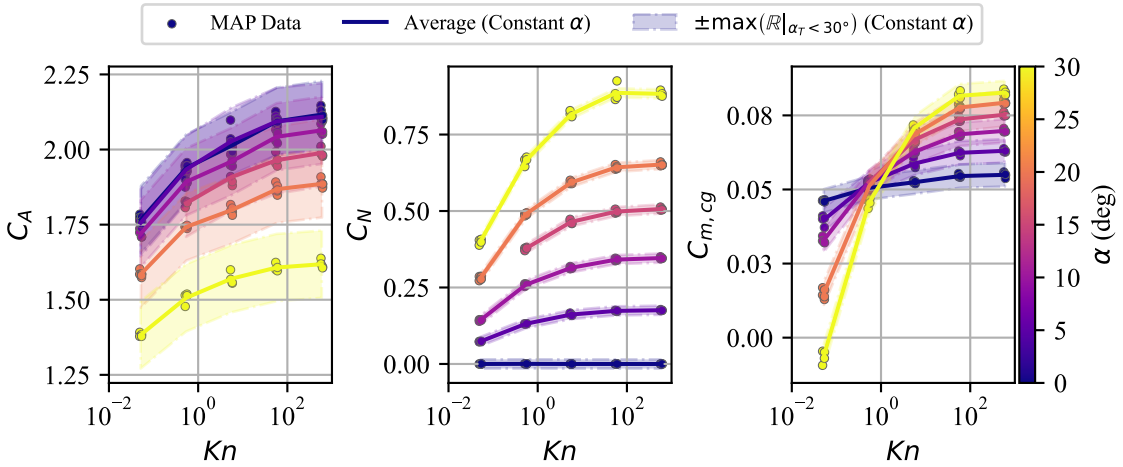

(b) Normal Force – Near-Trim Attitudes

Fig. 11 Reconciled Rarefied Aerodynamic Coefficients

2. Continuum

LAURA solutions in the current work were prescribed to investigate the sensitivity to velocity and total angle of attack. However, the data in Figure 10 suggest there is little variance in aerodynamic coefficients with respect to velocity for the considered flight envelope. This invariance is likely a result of asymptotic behavior in aerodynamic characteristics with respect to both Mach number and velocity, but was not investigated further in the current work. For that reason, reconciliation of the hypersonic continuum data instead used variation in coefficients with velocity to inform uncertainty of the coefficients, leaving total angle of attack as the sole independent variable of the reconciled coefficients. The mean value and uncertainty (3σ) were computed from the set of coefficients for all velocities and trajectories for each constant value of α_T. This reconciled data are shown in Figure 12.

B. Comparison to Mars Heritage Data

Considering the purpose of reusing a flight heritage vehicle design is to benefit from flying a known system, it is informative to compare the newly generated computational data against the heritage data to provide confirmation of data consistency with the assumed heritage. For this reason, the reconciled aerodynamic data and uncertainties from Section VI.A were compared with the underlying computational data which was used to build the aerodatabases for the predecessor Mars missions. The reconciled rarefied data for Uranus aerocapture conditions are compared against the available data from the Mars Exploration Rover (MER) EV [37] in Figure 13. It should be noted MER's DSMC data

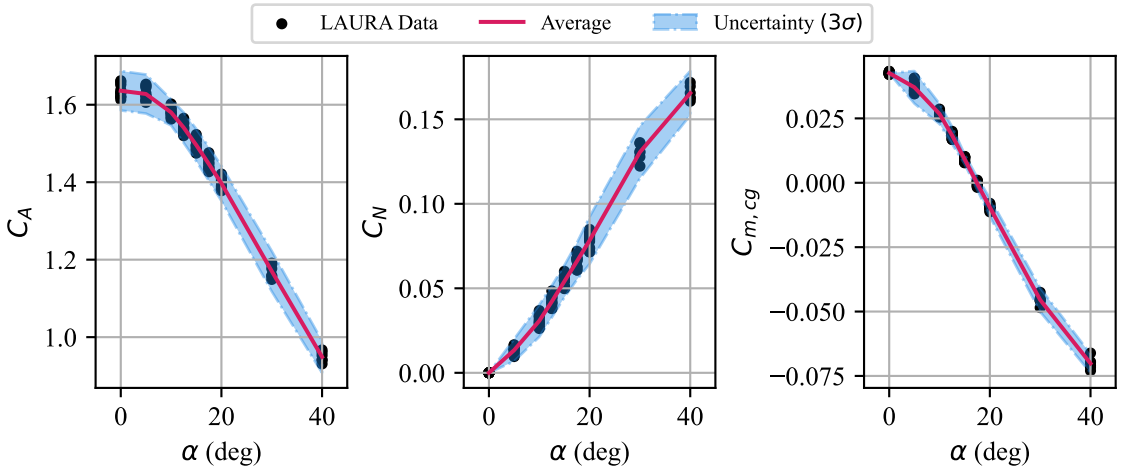

Fig. 12 Reconciled Hypersonic Continuum Aerodynamic Coefficients

were also used to formulate the rarefied aerodynamics modeling for MSL. This comparison shows good agreement for all but the lowest Kn data in each data set, where Uranus aerocapture data appears to continue dropping in magnitude with Kn while the MER data see a decrease in the local gradients. The exact cause of this deviation is difficult to determine due to the variety of different factors between the two data sets and the difficulty of properly converging DSMC solutions at low-Kn conditions where a large number of particles must be modeled. For these reasons, the cause of this difference was not further investigated in the current work. Future work would benefit from additional DSMC solutions prescribed to identify the cause of such differences. However, comparison of continuum data at even lower Kn can help inform whether this is the start of a trend or a singular point disagreement between datasets.

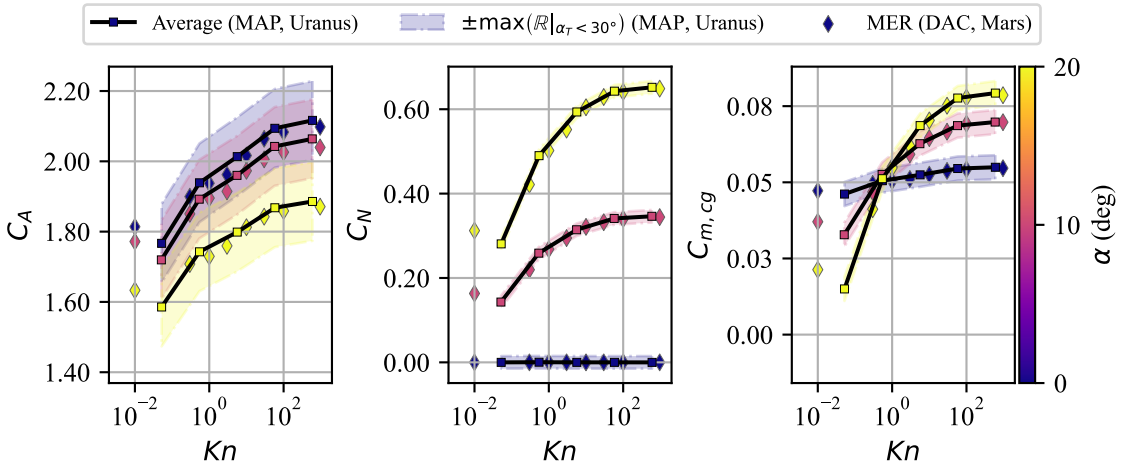

Fig. 13 Comparison of Uranus Rarefied Data to MER EV [37]

Reconciled continuum data and their uncertainties for Uranus aerocapture conditions are compared against the reported hypersonic continuum data of the MSL EV [21] in Figure 14. The MSL data were generated using the same LAURA forebody-only approach, similar to the Uranus methods. It is observed in this comparison that all MSL EV data appear to fit within the predicted uncertainty band for Uranus aerocapture conditions, even though the MSL EV data is for a much broader range of Mach numbers. Most importantly, the high-M data at values similar to that of Uranus aerocapture appear to show the best agreement with the reconciled nominal aerodynamic coefficients. This agreement strengthens the aerocapture system's tie to past missions. It also suggests the disagreement seen at $Kn \simeq 10^{-2}$ in the rarefied regime is localized, assuming the disagreement is rooted in physical differences between flight conditions.

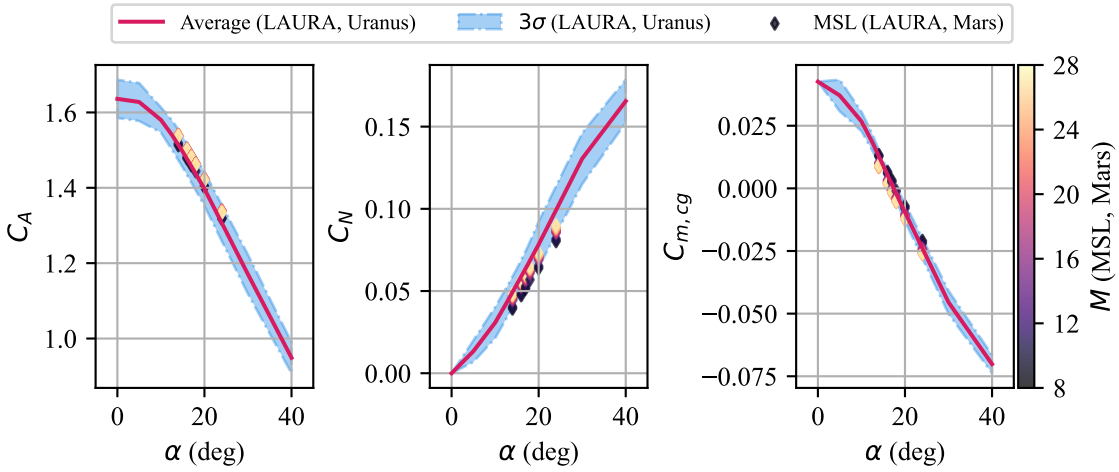

Fig. 14 Comparison of Continuum Hypersonic Data to MSL EV [21]

C. Nominal Aerodatabase

The reconciled aerodynamic data were used to populate an aerodynamic database for use in trajectory simulation, as the validation checks in Section VI.B were satisfactory for the current level of analysis. This database provides continuous aerodynamic coefficients across the foreseeable six degree-of-freedom (6-DoF) trajectory trade space to be utilized in mission design and optimization. Knudsen number and total angle of attack are the sampling variables for this aerodatabase. The discrete data were treated as anchor points. An interpolation function was used to smooth data output between anchor points.

At the free molecular bound ($Kn \gtrsim 10^3$), near exo-atmospheric maneuvering could orient the vehicle at much larger angles than it would see during the main aerocapture pass. For this reason, the database was populated up to larger total angles of attack to provide bounding data in this regime. Out-of-bounds detection was implemented for other regimes given the developmental and evolving nature of the current work to flag extrapolation from the underlying data. The output of the nominal aerodatabase is compared to the underlying data from Section V in Figure 15. The uncertainty modeling aspect of this aerodatabase is described in Section VII.

D. Sensitivity to Shape

Given the final 4.57 m configuration varies slightly from the 5 m scale MSL EV variant used to populate the aerodatabase detailed up to this point, understanding any variance between the two configurations was of interest. As noted in Section III, a similar growth was seen on MSL from the Viking heritage OML baseline and found to have no significant effects on the hypersonic aerodynamics. This assumption was revisited for the current work. Additional simulations were conducted to test for sensitivities to changes in the backshell OML. FUN3D was chosen for this analysis as the unstructured nature of the solver allows for much faster solution return times when compared to the need to build structured grids for each geometry, and was applied using the methods described in Section IV.C at the peak dynamic pressure condition. Three values were considered for the ratio of specific heats: 1.350, which is representative of the median value observed in LAURA simulations [14, 16], and 1.483 and 1.666, which are the pre- and post-shock values respectively as reported by NASA's Chemical Equilibrium Applications (CEA) tool [38] for a representative condition[‡]. Forces and moments were collected for each configuration, and Figure 16 shows the quantitative difference between configurations reported as the percent change observed from the 5 m scale MSL EV to the final modified 4.57 m configuration. The most significant change observed was to the normal force, which saw just under a 3% increase with the modified backshell. Pitching moment saw no more than a 1% increase, while axial force predicted an even smaller decrease of approximately 0.1% or less.

Changes to flow over the vehicles due to scale and backshell shape were also considered. Figures 17 and 18 plot coefficient contours of surface pressure and skin friction magnitude, respectively, on the two considered configurations.

[‡]It should be noted that the LAURA-matched ratio of specific heats value is considered the most accurate for the current application. While Uranus conditions push the limits of CEA's low-temperature capabilities, it is used in the current application as a method to obtain quick representative conditions for use analyzing first-order sensitivities.

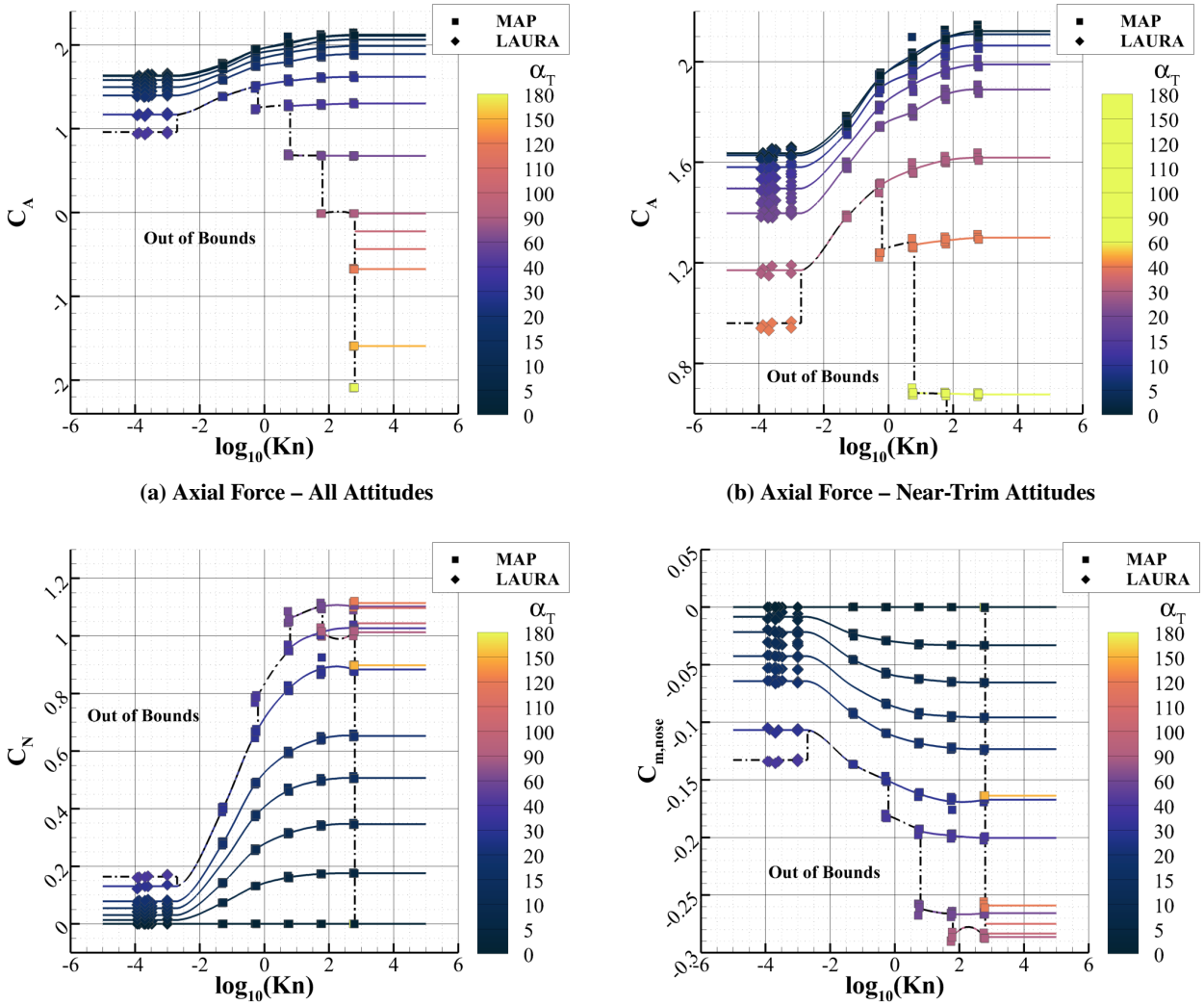

(a) Axial Force – All Attitudes

(b) Axial Force – Near-Trim Attitudes

(c) Normal Force – All Attitudes

(d) Pitching Moment – All Attitudes

Fig. 15 Nominal Aerodatabase and Underlying Data

The backshell contours are magnified relative to the heatshield and shoulder contours, 20x for pressure and 10x for skin friction magnitude, for ease of visual inspection due to the difference in scales across the vehicle. Coefficients are nondimensionalized according to the perfect gas conventions in FUN3D [36]. While there are no obvious large scale differences, subtle differences are apparent on closer inspection. The region of relatively-high pressure on the backshell shown in Figure 17(a) appears to grow with the expansion of the backshell in Figure 17(b). Similarly, the region of high skin friction magnitude also subtly appears to expand from Figure 18(a) to Figure 18(b). Both of these trends suggest increases in the attached flow on the the backshell, which was expected for the changes made. However, the observed changes do not present large deviations to the expected control of the vehicle for the aerodynamic performance modeling perspective, and any changes from the small increase to normal force are expected to improve aerocapture performance by adding control authority to the vehicle in lifting flight.

E. Dynamic Damping

For the current work, aerodynamics were assumed to be quasi-steady. This assumption was considered inherently conservative, as the MSL EV is dynamically stable in hypersonic continuum flight ($M \geq 5$) [39] and therefore removing the dynamic component terms only removes stabilizing damping moments from the model. Additional stability from damping may have second order consequences for the trade of vehicle stability and maneuverability, and should be

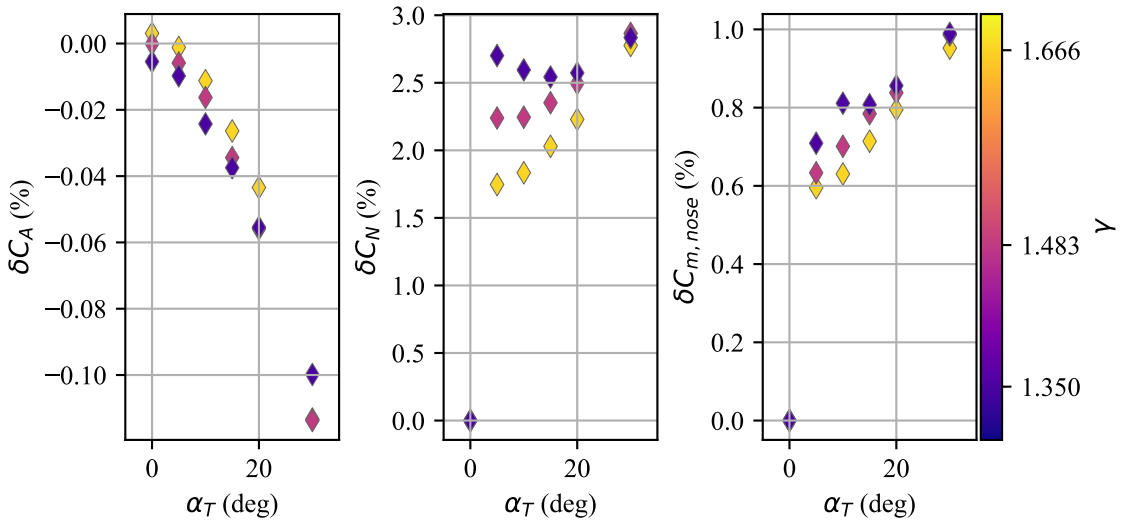

Fig. 16 FUN3D Backshell Sensitivity Study – Force and Moment Deltas with Effective-γ Effects

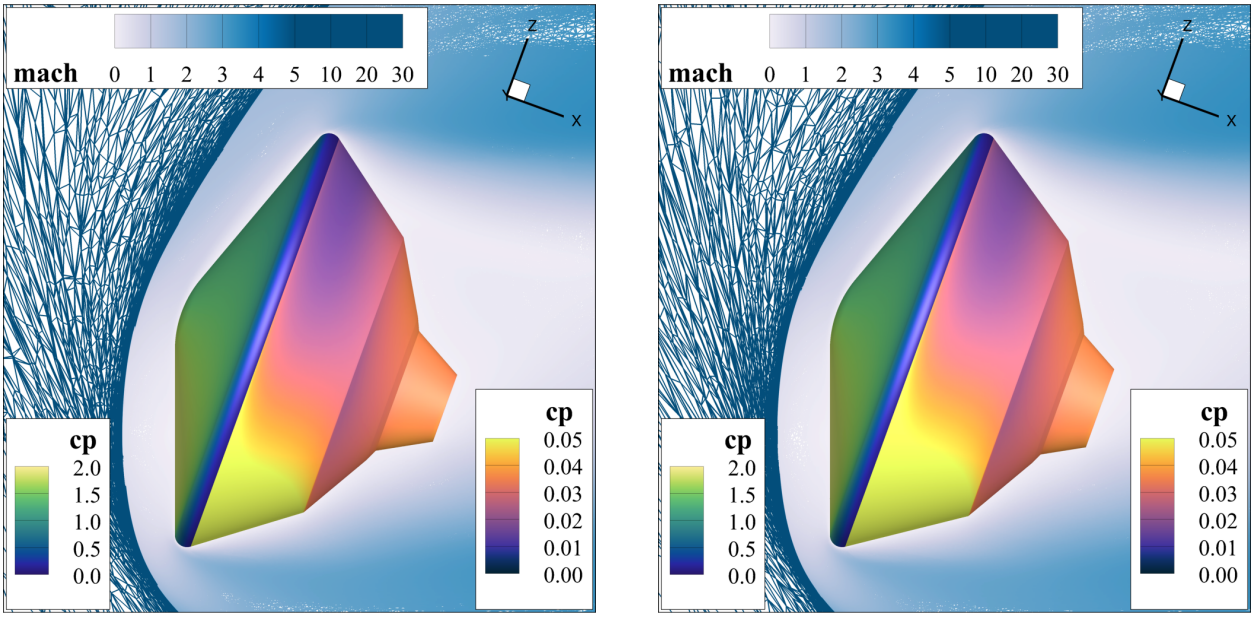

(a) 5.00 m Scale MSL with Original Backshell **(b) 4.57 m Scale MSL with Modified Backshell**

Fig. 17 FUN3D Backshell Sensitivity Study - Surface Pressure at Uranus Peak Dynamic Pressure, α_T = 20°

investigated in a more mature analysis. However, damping effects are expected to be small as the damping component of the moment scales proportional to $\dot{\theta}D/2\left|\vec{V}\right|$, where $\dot{\theta}$ is the dimensional rate, and due to the nature of aerocapture, the velocity term in the denominator is expected to be very large relative to the product of the angular rate and diameter in the numerator.

VII. Aerodynamic Uncertainties

With nominal aerodynamics assembled into an aerodatabase in Section VI, an associated uncertainty model can be formulated. One benefit of building from past planetary missions is that an uncertainty model has already been developed for the MSL EV. However, whether the uncertainty model is still valid must be considered. This section

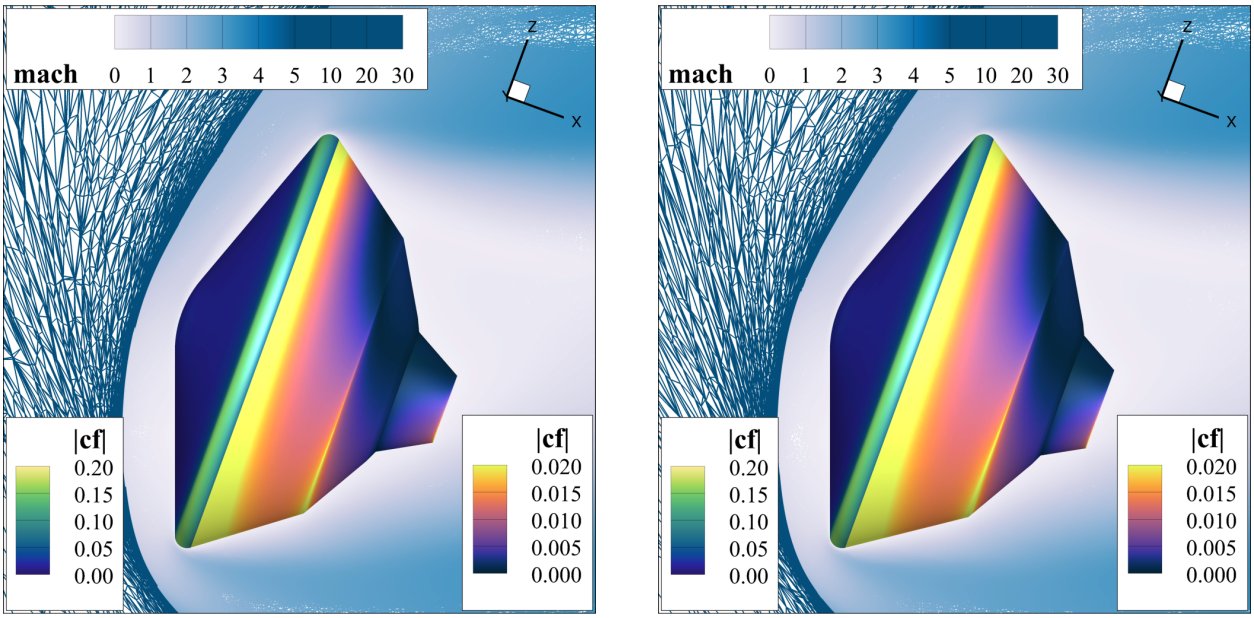

(a) 5.00 m Scale MSL with Original Backshell **(b) 4.57 m Scale MSL with Modified Backshell**

Fig. 18 FUN3D Backshell Sensitivity Study - Surface Friction at Uranus Peak Dynamic Pressure, $\alpha_T = 20°$

introduces the adopted uncertainty model from the MSL EV, investigates how the carried uncertainties compare to the newly generated data, and provides updates where appropriate to ensure the final uncertainty model is conservative given the early design nature of the current work. The flight performance of the nominal aerodatabase compiled in Section VI.C with the updated uncertainty model is presented.

A. MSL Uncertainty Model

The uncertainty model employed in the current work leverages the same methodology that was used for the MSL EV [10]. This uncertainty model builds off the experience of past planetary EDL missions to Mars, and was successfully used again for the Mars2020 flight [13]. The MSL EV uncertainty model uses the adder (U^A) and multiplier (U^M) terms, tabulated in Table 1, to augment the static force and moment coefficients through Equations 3 - 8. The coefficients are then dispersed through randomized factors applied to these adders and multipliers in a Monte Carlo analysis.

Table 1 MSL EV 3σ Aerodynamic Uncertainties

	C_A	C_Y, C_N	C_m	C_n	C_l
$Kn > 0.1$	±5%	±0.01, ±10%	±0.005, ±20%	±0.005, ±20%	0.0005
$M > 10$	±3%	±0.01, ±10%	±0.006, ±20%	±0.003, ±20%	0.000219

$$C_{A_{disp}} = C_A(\alpha,\beta)\left(1 + U^M_{C_A}\right) \tag{3}$$

$$C_{Y_{disp}} = \left[C_Y(\alpha,\beta) + U^A_{C_Y}\right]\left(1 + U^M_{C_Y}\right) \tag{4}$$

$$C_{N_{disp}} = \left[C_N(\alpha,\beta) + U^A_{C_N}\right]\left(1 + U^M_{C_N}\right) \tag{5}$$

$$C_{l_{disp}}\Big|_{cg} = \frac{\Delta y}{D}C_N(\alpha,\beta) - \frac{\Delta z}{D}C_Y(\alpha,\beta) + U^A_{C_l} \tag{6}$$

$$C_{m_{disp}}\Big|_{cg} = \left[C_m(\alpha,\beta) + \frac{\Delta x}{D}C_N(\alpha,\beta) - \frac{\Delta z}{D}C_A(\alpha,\beta) + U^A_{C_m}\right]\left(1 + U^M_{C_m}\right) \tag{7}$$

$$C_{n_{disp}}\Big|_{cg} = \left[C_n(\alpha,\beta) + \frac{\Delta x}{D}C_Y(\alpha,\beta) - \frac{\Delta y}{D}C_A(\alpha,\beta) + U^A_{C_n}\right]\left(1 + U^M_{C_n}\right) \tag{8}$$

Early investigations of the current work used this uncertainty model as is [14]. However, for a more robust analysis, it must be questioned whether the assumptions of this uncertainty model, developed for flight at the CO_2-dominant atmosphere of Mars, still hold for the H_2, He dominant atmosphere of Uranus. For example, while the MSL EV uncertainties were based on prior Mars missions, $U^A_{C_m}$ was doubled due to sensitivities to modeled gas chemistry and reaction rate effects of flight in Mars atmosphere [10]. While data to gauge similar effects for the new considerations brought by flight in H_2, He are limited at present, the available data from Section VI can be used to provide a first order analysis. The hypersonic continuum regime was the flight segment of most interest for this analysis, as this is where the vehicle sees the most deceleration and control authority for guidance through the aerocapture maneuver. A comparison of the computational data uncertainty from the current work with the $\pm 3\sigma$ bounds of the MSL uncertainties, presented in Figure 19, indicates the observed uncertainty in the current hypersonic data formulation accounts for the entirety of the modeled uncertainty for C_A, the majority of uncertainty carried for C_N, and a sizeable portion for $C_{m,cg}$. For this reason, an update to the MSL uncertainties to provide more conservative bounds to Uranus aerocapture was devised.

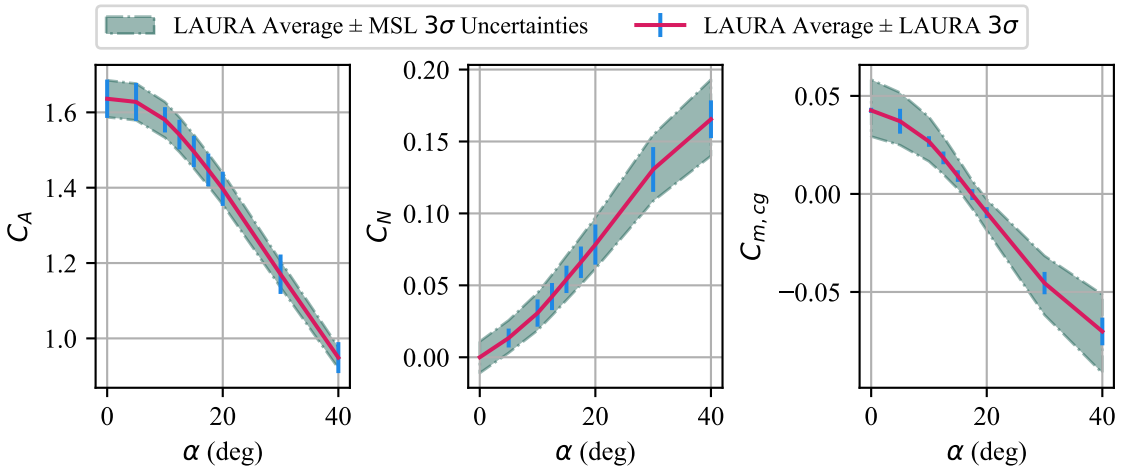

Fig. 19 LAURA Computation Uncertainties Only vs MSL Heritage Model

B. Updates for Uranus Aerocapture Applications

The uncertainty quantification presented in Section VI.A were used to update the MSL uncertainty model to better encompass the observed uncertainties for Uranus aerocapture conditions. A root-sum-square (RSS) process was used to combine the heritage MSL uncertainties with the uncertainties associated with the new data for Uranus conditions, as a direct sum would likely result in over-conservatism through duplication of captured uncertainty sources in the model. For axial force, which only carries a multiplier uncertainty term, $U^M_{C_A}$ was updated proportionally to U_{C_A}/C_A. For the remaining force and moment coefficients, the respective adder uncertainties (U^A) were updated directly with the carried uncertainties. The multipliers, which are intended to capture slope uncertainties for terms like $\partial C_N/\partial\alpha$ and $\partial C_m/\partial\alpha$, were not updated in cases where adders could be to avoid duplication of uncertainties.

These updates were made for both continuum and rarefied aerodynamics uncertainties for consistency, and the updated uncertainty terms are presented in Table 2. The comparison of this updated uncertainty model and the observed uncertainty of flight conditions in the current work is shown in Figure 20, which shows the RSS update successfully adds margin to ensure a bounding uncertainty model. To provide context to these updated uncertainties, the effect on the nominal flight trajectory is presented in the following section.

Table 2 Updated 3σ Aerodynamic Uncertainties for Uranus Aerocapture

	C_A	C_Y, C_N	C_m	C_n	C_l
$Kn > 0.1$	±7.45%	±0.0179, ±10%	±0.00652, ±20%	±0.00596, ±20%	0.0005
$M > 10$	±5.38%	±0.0185, ±10%	±0.00948, ±20%	±0.00693, ±20%	0.000219

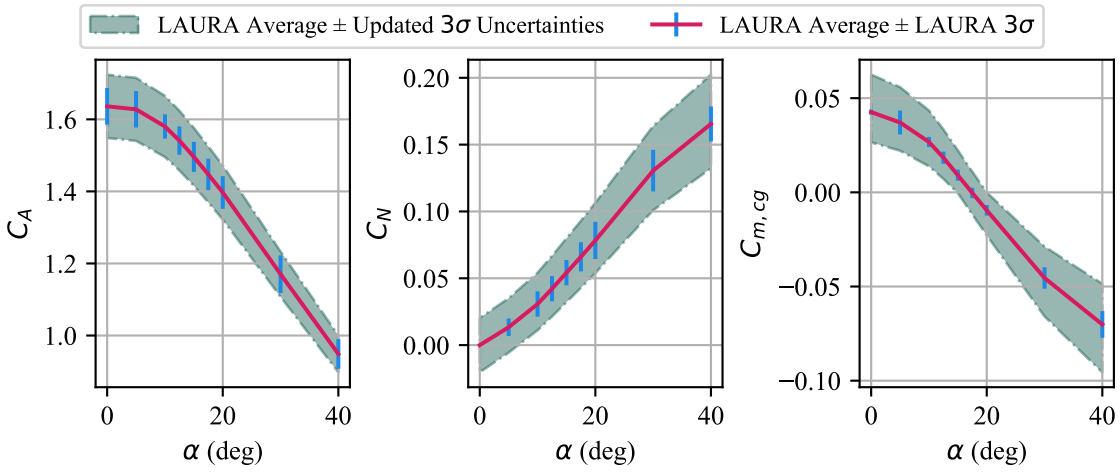

Fig. 20 Updated Continuum Uncertainties from LAURA Solutions

C. Impacts on Flight Trajectory

Figure 21 shows the -3σ (0.13 %-tile), +3σ (99.87 %-tile), and mean aerocapture trajectories arising from 6-DoF Monte Carlo simulation runs. More information on the setup of the 6-DoF simulation framework can be found in Reference [40]. The aerodynamic force and moment coefficients that are simulated in the aerodatabase are shown in the figure. Vertical lines in magenta show critical Knudsen numbers, which illustrate the trajectory traversing flow regimes from free-molecular to transitional to continuum to transitional and finally to free-molecular. Inertial flight path angle is chosen as the independent variable in the plots to illustrate the trajectory descending (e.g. negative angles) and ascending (e.g. positive angles) in the atmosphere. Vertical grey lines show critical events in the aerocapture trajectory, including atmosphere entry/exit, guidance on/off, and periapsis (minimum altitude).

Figure 22 illustrates the statistical uncertainty affect on aerocapture performance, including the lift-to-drag ratio and trajectory-space. In the region of active guidance (e.g. hypersonic continuum), the aeroshell is able to nominally trim and hold the desired L/D of 0.25. With aerodynamic uncertainties applied, the achieved trim L/D ranges from 0.2 to 0.3 (±20% increase/decrease). This aerodynamic uncertainty was shown to influence the aerocapture trajectory the most once guidance initiates in continuum regime. The trajectory "corridor" that the uncertainty bounds define grows up until guidance shutoff. On the ascending traverse through the transitional and free-molecular flow regimes, the "corridor" width remains the same. Nevertheless, the aerocapture vehicle retains sufficient control margin to statistically achieve orbital capture despite the affects of aerodynamic uncertainity propagated throughout atmospheric flight.

VIII. Conclusion

The application of the MSL (and Mars 2020) EV geometry for use as an aerocapture system to deliver a flagship-class planetary science mission to Uranus has been investigated. In support of this effort, a new aerodynamic database has been developed for simulating flight in a broad range of relevant conditions for such a mission in a H_2, He dominant atmosphere. This aerodatabase is based on computational data, obtained from MAP DSMC and LAURA CFD solutions which were used to formulate nominal aerodynamic characteristics. These data show good agreement with characteristics of past vehicles which flew successfully at Mars despite atmospheric differences.

Variation in the new computational data for Uranus aerocapture conditions has been used to update the pre-existing uncertainty model from the MSL EV to better bound potential variations of aerodynamic characteristics during flight through Uranus' atmosphere. While some modifications to the MSL EV design were required to close the design for

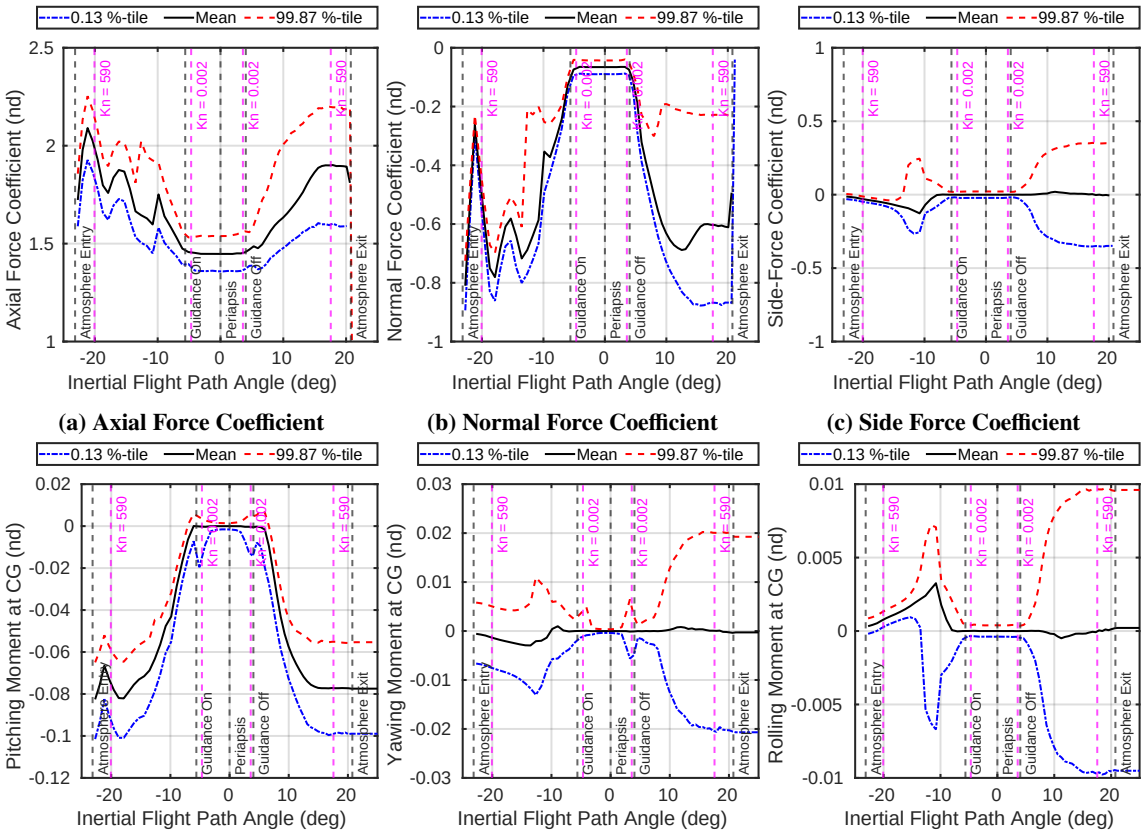

(a) Axial Force Coefficient **(b) Normal Force Coefficient** **(c) Side Force Coefficient**

(d) Pitching Moment at C.G. **(e) Yawing Moment at C.G.** **(f) Rolling Moment at C.G.**

Fig. 21 Aerodynamic Force/Moment Coefficient Uncertainties Applied to Aerocapture Trajectory

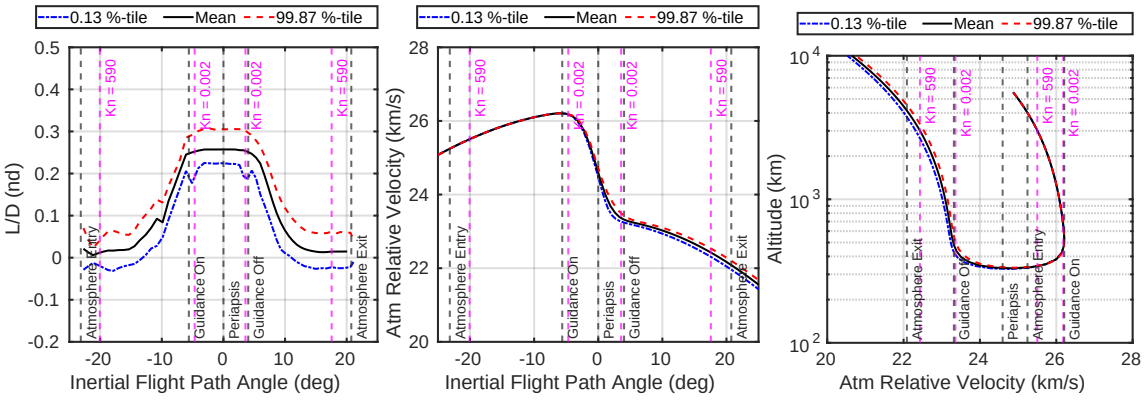

(a) Lift-To-Drag Ratio **(b) Velocity-FPA Space** **(c) Velocity-Altitude Space**

Fig. 22 Statistical View of Aerodynamic Uncertainty Applied to Aerocapture Trajectory

aspects outside of aerodynamics, CFD analysis in FUN3D has shown that these differences were minor, and within the uncertainty ranges. Flight trajectory analysis has shown that despite increasing the uncertainty associated with the geometry, the system was still able to maintain sufficient control margins to accomplish mission objectives.

The current work provides a model which is adequate for early mission design work. If such a mission as described were to proceed, future work would focus on refining these models to further encompass the potential flight trajectory space and look for any higher order effects which may not be captured in the current analysis. While current data suggest the presented uncertainty model based on the MSL EV and additional Uranus-specific computational data is bounding,

for a flagship mission, it would be desirable to revisit this assumption and build up an uncertainty model specifically intended for Uranus' atmosphere, rather than re-purposing one developed for Mars applications. It should also be noted that the current work is limited to primarily considering aleatoric uncertainty sources in the computational models. Epistemic uncertainty sources, such as the accuracy of the underlying gas models for H_2 and He gas compositions, pose additional challenges that could introduce further uncertainty to the analysis. For this reason, increased availability of validation data (such as shock tube experiments) for H_2, He computational methods would also benefit future work.

Acknowledgments

The work presented in this paper was funded by the Ice Giant Aerocapture Early Career Initiative project sponsored by the NASA Space Technology Mission Directorate. Computing resources supporting this work were provided by the K Cluster at NASA Langley Research Center. The authors would like to thank the project mentors at NASA Langley Research Center, NASA Ames Research Center, and the Jet Propulsion Laboratory. Much gratitude is owed to Neil Cheatwood, Karl Edquist, Mark Schoenenberger, and Ashley Korzun for many discussions on the formulation of the newly developed or expanded models presented in the current work, and to Derek Liechty for guidance in configuring the MAP solver for the presented work. Additionally, the authors would like to thank Ron Neale for creating the aerocapture concept of operations graphic presented in Figure 1.

References

[1] "Origins, Worlds, and Life: A Decadal Strategy for Planetary Science and Astrobiology 2023-2032," Tech. rep., The National Academies Press, 2022. https://doi.org/10.17226/26522.

[2] Simon, A., Nimmo, F., and Anderson, R., "Uranus Orbiter and Probe: Journey to an Ice Giants System," Tech. rep., National Aeronautics and Space Administration, 2021.

[3] Dutta, S., Perez-Ayucar, M., Fedele, A., Gardi, R., Calabuig, G. D., Schuster, S., Lebreton, J.-P., Ali, H. K., Sayanagi, K., Ozmen, I. S., Reimer, T., Sotin, C., Scully, J., Lu, Y., Reddy, S. A., Arnold, J. O., Feldman, J., Jha, V., Wright, M., Hill, J. P., Ellerby, D. T., Wilder, M., Alunni, A., D'Souza, S., Johnson, B., Sostaric, R. R., Matz, D. A., Moses, R. W., Young, C., Girija, A. P., Saikia, S. J., Lu, P., Hormigo, T., Afonso, G., Jelloian, C., Albert, S. W., Hume, S., Bailet, G., Putnam, Z., Falcone, G., Kluever, C., Rea, J. R., Cohen, I. J., Trawny, N., Chen, G. T., Spencer, D. A., Allen, G. A., Dillman, R., Austin, A., Venkatapahty, E., Munk, M., Cutts, J. A., Lobbia, M. A., Nelessen, A. P., Bhaskaran, S., Powell, R., Deshmukh, R., Tackett, B., Wercinski, P., Lugo, R., and Cassell, A. M., "Aerocapture as an Enhancing Option for Ice Giants Missions," *Bulletin of the AAS*, Vol. 53, No. 4, 2021. URL https://baas.aas.org/pub/2021n4i046.

[4] Girija, A., "A Flagship-class Uranus Orbiter and Probe mission concept using aerocapture," *Acta Astronautica*, Vol. 202, 2022, pp. 104–118. https://doi.org/10.1016/j.actaastro.2022.10.005.

[5] Dutta, S., Shellabarger, E., Scoggins, J. B., Gomez-Delrio, A., Lugo, R., Deshmukh, R., Tackett, B., Williams, J., Johnson, B., Matz, D., Geiser, J., Morgan, J., Restrepo, R., and Mages, D., "Uranus Flagship-class Orbiter and Probe Using Aerocapture," *AIAA SciTech 2024 Forum*, Orlando, FL, 2024. https://doi.org/10.2514/6.2024-0714, URL https://arc.aiaa.org/doi/abs/10.2514/6.2024-0714.

[6] Restrepo, R., Mages, D., Smith, M., Deshmukh, R., Dutta, S., and Benhacine, L., "Mission Design and Navigation Solutions for Uranus Aerocapture," *AIAA SciTech 2024 Forum*, Orlando, FL, 2024. https://doi.org/10.2514/6.2024-0715, URL https://arc.aiaa.org/doi/abs/10.2514/6.2024-0715.

[7] Lockwood, M., "Aerocapture Systems Analysis for a Neptune Mission," Tech. rep., NASA TM 2006-214300, 2006.

[8] Edquist, K., Prabhu, R., Hoffman, D., and Rea, J., "Configuration, Aerodynamics, and Stability Analysis for a Neptune Aerocapture Orbiter," *AIAA Atmospheric Flight Mechanics Conference and Exhibit*, 2004. https://doi.org/10.2514/6.2004-4953, URL https://arc.aiaa.org/doi/abs/10.2514/6.2004-4953.

[9] Seiff, A., Venkatapathy, E., Haas, B., and Intrieri, P., "Galileo Probe Aerodynamics," *AIAA 14th Applied Aerodynamics Conference*, 1996. https://doi.org/10.2514/6.1996-2451, URL https://arc.aiaa.org/doi/abs/10.2514/6.1996-2451.

[10] Schoenenberger, M., Dyakonov, A., Buning, P., Scallion, W., and Norman, J. V., "Aerodynamic Challenges for the Mars Science Laboratory Entry Descent and Landing," *41st AIAA Thermophysics Conference*, 2009. https://doi.org/10.2514/6.2009-3914, URL https://arc.aiaa.org/doi/abs/10.2514/6.2009-3914.

[11] Schoenenberger, M., Norman, J. V., Karlgaard, C., Kutty, P., and Way, D., "Assessment of the Reconstructed Aerodynamics of the Mars Science Laboratory Entry Vehicle," *Journal of Spacecraft and Rockets*, Vol. 51, No. 4, 2014, pp. 1076–1093. https://doi.org/10.2514/1.A32794, URL https://doi.org/10.2514/1.A32794.

[12] Dutta, S., Way, D. W., Zumwalt, C. H., and Blette, D. J., "Postflight Assessment of Mars 2020 Entry, Descent, and Landing Simulation," *Journal of Spacecraft and Rockets*, Vol. 61, No. 3, 2024, pp. 847–857. https://doi.org/10.2514/1.A35771, URL https://doi.org/10.2514/1.A35771.

[13] Karlgaard, C. D., Schoenenberger, M., Dutta, S., and Way, D. W., "Mars Entry, Descent, and Landing Instrumentation 2 Trajectory, Aerodynamics, and Atmosphere Reconstruction," *Journal of Spacecraft and Rockets*, Vol. 60, No. 1, 2023, pp. 199–214. https://doi.org/10.2514/1.A35440, URL https://doi.org/10.2514/1.A35440.

[14] Shellabarger, E. R., Scoggins, J., Hinkle, A. D., Dutta, S., Deshmukh, R. G., Patel, M., and Agam, S., "Aerodynamic Implications of Aerocapture Systems for Uranus Orbiters," *AIAA SciTech 2024 Forum*, Orlando, FL, 2024. https://doi.org/10.2514/6.2024-0950, URL https://arc.aiaa.org/doi/abs/10.2514/6.2024-0950.

[15] Gomez-Delrio, A. J., and Dutta, S., "Design Implications for Aerocapture Systems Placing Flagship-class Uranus Orbiters," *AIAA SciTech 2024 Forum*, Orlando, FL, 2024. https://doi.org/10.2514/6.2024-0953, URL https://arc.aiaa.org/doi/abs/10.2514/6.2024-0953.

[16] Scoggins, J. B., Hinkle, A. D., and Shellabarger, E. R., "Aeroheating Environment of Aerocapture Systems for Uranus Orbiters," *AIAA SciTech 2024 Forum*, Orlando, FL, 2024. https://doi.org/10.2514/6.2024-0951, URL https://arc.aiaa.org/doi/abs/10.2514/6.2024-0951.

[17] Morgan, J., Williams, J., Venkataphy, E., Gasch, M., Deshmukh, R., Shellabarger, E., Scoggins, J. B., Gomez-Delrio, A. J., Tackett, B., and Dutta, S., "Thermal Protection System Design of Aerocapture Systems for Uranus Orbiters," *AIAA SciTech 2024 Forum*, Orlando, FL, 2024. https://doi.org/10.2514/6.2024-0952, URL https://arc.aiaa.org/doi/abs/10.2514/6.2024-0952.

[18] Dutta, S., Davis, W., Deshmukh, R., Gomez-Delrio, A., Lugo, R., Scoggins, J., Shellabarger, E., Chadalavada, P., Garland, J., Williams, J., Morgan, J., Mages, D., Restrepo, R., Johnson, B., Matz, D., and Sandoval, S., "Aerocapture Solutions for Flagship-class Uranus Orbiter and Probe," *2025 AIAA SciTech Conference,* Orlando, FL, 2025.

[19] Gomez-Delrio, A., Davis, W., Deshmukh, R., and Dutta, S., "Design Considerations for Aerocapture Delivery of Uranus Orbiter and Probe," *2025 AIAA SciTech Conference,* Orlando, FL, 2025.

[20] Kirk, D. B., Intrieri, P. F., and Seiff, A., "Aerodynamic Behavior of the Viking Entry Vehicle: Ground Test and Flight Results," *Journal of Spacecraft and Rockets*, Vol. 15, No. 4, 1978. https://doi.org/10.2514/3.57307, URL https://doi.org/10.2514/3.57307.

[21] Dyakonov, A., Schoenenberger, M., and Norman, J. V., "Hypersonic and Supersonic Static Aerodynamics of Mars Science Laboratory Entry Vehicle," *43rd AIAA Thermophysics Conference*, 2012. https://doi.org/10.2514/6.2012-2999, URL https://arc.aiaa.org/doi/abs/10.2514/6.2012-2999.

[22] Liechty, D. S., "Object-Oriented/Data-Oriented Design of a Direct Simulation Monte Carlo Algorithm," *Journal of Spacecraft and Rockets*, Vol. 52, No. 6, 2015, pp. 1521–1529. https://doi.org/10.2514/1.A33177, URL https://doi.org/10.2514/1.A33177.

[23] Swaminathan-Gopalan, K., "Consistent treatment of transport properties of weakly-ionized gas mixtures in DSMC," Master's thesis, University of Illinois at Urbana-Champaign, 2015. URL https://hdl.handle.net/2142/89077.

[24] Justh, H., Dwyer Cianciolo, A. M., Hoffman, J., and Jr., G. A., "Uranus Global Reference Atmospheric Model (Uranus-GRAM): User Guide," Technical Memorandum NASA TM-20210017250, NASA June 2021. URL https://ntrs.nasa.gov/citations/20210017250.

[25] Gnoffo, P. A., "An Upwind-Biased, Point-Implicit Relaxation Algorithm for Viscous, Compressible Perfect-Gas Flows," TP 2953, NASA, 1990.

[26] Thompson, K. B., Johnston, C. O., Hollis, B. R., and Lessard, V. R., "Recent Improvements to the LAURA and HARA Codes," AIAA Paper 2020-3030, June 2020.

[27] Thompson, K., Hollis, B. R., Johnston, C. O., Kleb, B., Lessard, V., and Mazaheri, A., "LAURA Users Manual v5.6," TM 2020-220566, NASA, 2020.

[28] Johnston, C. O., "Nonequilibrium Shock-Layer Radiative Heating for Earth and Titan Entry," Ph.D. thesis, Virginia Polytechnic Institute and State University, 2006.

[29] Gnoffo, P. A., Gupta, R. N., and Shinn, J. L., "Conservation Equations and Physical Models for Hypersonic Air Flows in Thermal and Chemical Nonequilibrium," TP 2867, NASA, 1989.

[30] Yee, H. C., "On symmetric and upwind TVD schemes," TM 1985-86842, NASA, 1985.

[31] Johnston, C. O., and Mazaheri, A., "Impact of Non-Tangent-Slab Radiative Transport on Flowfield-Radiation Coupling," *Journal of Spacecraft and Rockets*, Vol. 455, No. 4, 2018. https://doi.org/10.2514/1.A34072.

[32] Park, C., Jaffe, R. L., and Partridge, H., "Chemical-Kinetic Parameters of Hyperbolic Earth Entry," *Journal of Thermophysics and Heat Transfer*, Vol. 15, No. 1, 2001, pp. 76–90. https://doi.org/10.2514/2.6582, URL https://doi.org/10.2514/2.6582.

[33] Fujita, K., Yamada, T., and Ishii, N., "Impact of Ablation Gas Kinetics on Hyperbolic Entry Radiative Heating," *44th AIAA Aerospace Sciences Meeting and Exhibit*, 2006. https://doi.org/10.2514/6.2006-1185, URL https://arc.aiaa.org/doi/abs/10.2514/6.2006-1185.

[34] Kleb, W. L., Park, M. A., Wood, W. A., Bibb, K. L., Thompson, K. B., and Gomez, R. J., "Sketch-to-Solution: An Exploration of Viscous CFD with Automatic Grids," *AIAA Aviation 2019 Forum*, 2019. https://doi.org/10.2514/6.2019-2948, URL https://arc.aiaa.org/doi/abs/10.2514/6.2019-2948.

[35] Pederson, C., and Schoenenberger, M., "Exploring the Accuracy of RANS Simulations for Mars Entry Vehicles," *AIAA Aviation 2023 Forum*, 2023. https://doi.org/10.2514/6.2023-3695, URL https://arc.aiaa.org/doi/abs/10.2514/6.2023-3695.

[36] Anderson, W. K., Biedron, R. T., Carlson, J.-R., Derlaga, J. M., Druyor, C. T., Gnoffo, P. A., Hammond, D. P., Jacobson, K. E., Jones, W. T., Kleb, B., Lee-Rausch, E. M., Nastac, G. C., Nielsen, E. J., Park, M. A., Rumsey, C. L., Thomas, J. L., Thompson, K. B., Walden, A. C., Wang, L., Wood, S. L., Wood, W. A., Diskin, B., Liu, Y., and Zhang, X., "FUN3D Manual: 14.0.1," Technical Memorandum NASA TM–20230004211, NASA Langley Research Center, April 2023. URL https://ntrs.nasa.gov/citations/20230004211.

[37] Schoenenberger, M., Cheatwood, F. M., and Desai, P., "Static Aerodynamics of the Mars Exploration Rover Entry Capsule," *43rd AIAA Aerospace Sciences Meeting and Exhibit*, 2005. https://doi.org/10.2514/6.2005-56, URL https://arc.aiaa.org/doi/abs/10.2514/6.2005-56.

[38] McBride, B. J., and Gordon, S., "Computer Program for Calculation of Complex Chemical Equilibrium Compositions and Applications," RP 1311, NASA, 1996.

[39] Schoenenberger, M., Yates, L., and Hathaway, W., "Dynamic Stability Testing of the Mars Science Laboratory Entry Capsule," *41st AIAA Thermophysics Conference*, 2009. https://doi.org/10.2514/6.2009-3917, URL https://arc.aiaa.org/doi/abs/10.2514/6.2009-3917.

[40] Deshmukh, R., Dutta, S., and Chadalavada, P., "6-DOF Uranus Aerocapture Trajectory Analysis," *2025 AIAA SciTech Conference,* Orlando, FL, 2025.